BIPOLAR MAGNETOPHORETIC SYSTEM FOR THE MANIPULATION OF MAGNETIC PARTICLES

Andrei AVRAM[1], Cătălin TIBEICĂ[2], Cătălin MĂRCULESCU[3], Marius VOLMER[4], Marioara AVRAM[5], Horia GAVRILĂ[6]

The paper presents the fabrication of an active bipolar magnetophoretic system, composed of parallel conductive wires embedded in the sidewalls of a microfluidic channel. Basic characterization was obtained by performing electromagnetic and electrothermal simulations, to determine the generated magnetic field as well as the temperature variations. Experiments were carried out using a solution of maghemite superparamagnetic nanoparticles suspended in deionized water. The experimental results prove the ability of the system to trap and manipulate the magnetic particles.

Keywords: magnetophoresis, active magnetophoretic system, microfluidics

1. Introduction

Magnetophoresis is the movement induced by the magnetic field to a particle in suspension [1]. It has been long used in the mining industry for separating iron ore [2]. Starting with the '90s, magnetophoretic systems have been employed in the separation of biological cells [3].

Magnetic Activated Cell Sorting (MACS) is one of the most widely spread technique for manipulating and sorting biological cells from complex flows. The technique is based on selective binding of magnetic particles to target cells, which are then extracted by magnetic field gradients [4,5]. It is very useful for processing high volumes in a short period of time [6].

[1] Phys., Laboratory for Micro- and Nano- Fluidics, National Institute for R&D in Microtechnology – IMT Bucharest, Romania; PhD student at the Faculty of Electrical Engineering, University POLITEHNICA of Bucharest, Romania e-mail: andrei.avram@imt.ro

[2] Phys, Simulation, Modelling and Computer-Aided Design Laboratory, National Institute for R&D in Microtechnology – IMT Bucharest, Romania, e-mail: catalin.tibeica@imt.ro

[3] PhD eng., Laboratory for Micro- and Nano- Fluidics, National Institute for R&D in Microtechnology – IMT Bucharest, Romania, e-mail: catalin.marculescu@imt.ro

[4] PhD eng., Department of Electrical Engineering and Applied Physics, "Transilvania" University of Brasov, e-mail: volmerm@unitbv.ro

[5] PhD eng., Laboratory for Micro- and Nano- Fluidics, National Institute for R&D in Microtechnology – IMT Bucharest, Romania, e-mail: marioara.avram@imt.ro

[6] Prof., Laboratory of Technical Magnetism, Faculty of Electrical Engineering, University POLITEHNICA of Bucharest, Romania, e-mail: horia.gavrila@upb.ro

The first microfluidic systems with integrated magnetic structures were published by Chong H. Ahn and Mark G. Allen in 1994 [7], and consisted of two copper coils with a permalloy core fabricated on the bottom of a fluidic microchannel. The design was later improved by adding an electrochemical sensor, turning this active magnetophoretic system into one of the first lab on chip systems [8]. Several research groups continued to develop the concept by further integration and miniaturization of the electromagnets [9,10] and by experimenting with active [11] or passive [12] magnetophoretic systems. Magnetophoresis systems have proven their strength over the past decade, different groups showing the ability to separate biological cells [13], manipulate magnetic particles [14], and enhance microfluidic mixing [15]. Recently, further developments in microfluidics and magnetophoretic systems allowed the integration with complex electronics, employing spin valve arrays [16], or planar Hall sensors [17].

The paper presents the fabrication of a bipolar active magnetophoretic system, which allows the generation of magnetic fields on the chip. The magnetic field gradient is obtained by applying small currents to electrical conductive wires embedded in the side walls of the microchannel, thus the wires are brought as close as possible to the fluid flow, the insulating layer being only 0.5 μm thick. The embedded wires run parallel to each other and to the flow direction, creating a magnetic field gradient from the center of the channel towards the edges.

The fabrication techniques involved in the fabrication of the system are ICT (Integrated Circuits Technology) compatible, allowing for further integration with electronic systems. The device was simulated in COMSOL Multiphysics to determine the magnetic field inside the microfluidic channel as well as the heat generated by the conductive wires. In order to prove the ability of the device to trap and manipulate magnetic particles, a solution of maghemite superparamagnetic nanoparticles was flown through the system, and the separation from the solution was observed.

The novelty of the device consists in the integration of conductive wires in the sidewalls of the microfluidic channels. This bipolar system allows further improvements by adding multiplying the number conductive wires which generate the magnetic field, turns the system into a tri-pole, quadripole, and so on.

2. The fabrication of the magnetophoretic device

The fabrication starts from a <100> silicon wafer on which a 500 nm thick silicon oxide layer is grown. This layer serves as an electrical insulator between the conductive wires, which will be patterned later, and the silicon substrate. After oxidation, the metal layers are deposited by DC sputtering in the AUTO500 system (Edwards, UK). First, an adhesion 30 nm chromium layer is deposited, followed by the deposition of a 300 nm gold layer.

For the patterning of the metal layers, the wafer surface was spin coated HPR 504 photoresist and exposed through a photolithographic mask. Fig. 1 shows the CleWin design of the metal pattern. The width of the wires is 20 μm (in the thinnest section) and the spacing between the two parallel wires is 20 μm.

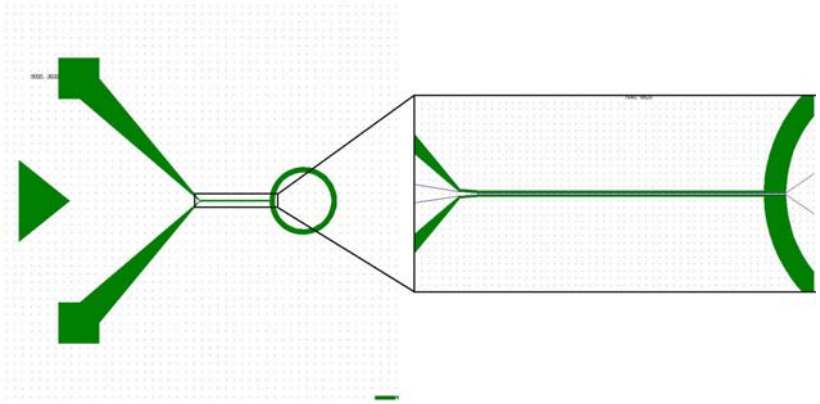

Fig. 1: The pattern of the metal layers. On the left, a detail showing the area of interest

After the wet etching of the Cr/Au metal layer, the wafer was rinsed in deionized (DI) water and washed in acetone and isopropyl alcohol (IPA). This cleaning step prepares the wafer for the passivation of the metal layers. Before the deposition of the oxide insulating layer, the wafer is exposed for 10 minutes to oxygen plasma in the SI 220 reactive ion etching system (Sentech Instruments, Germany). This ensures all organic contaminants from the cleaning step are efficiently removed from the surface, allowing the passivation layer to form a good contact with the metal layers. A thin 500 nm layer of SiO_2 was deposited in a Plasma Enhanced Chemical Vapor Deposition system (SPTS, UK), in order to passivate the metal layers. As gold starts the diffusion at about 300^{o}C, the deposition was performed at a safe temperature of 200^{o}C. The deposition took place from the reaction of silane (SiH_4) and nitrous oxide (N_2O) diluted with N_2 gas.

The microfluidic channel was fabricated in the reactive ion etching system, using HPR 504 photoresist as an etch mask. The process required a special chemistry using trifluoromethyl gas (CHF_3) diluted with argon (Ar). This process was developed to obtain a perfect anisotropic etching process of the PECVD and thermal silicon oxides previously deposited.

Next, the front of the wafer was covered with a thin layer of photoresist in order to protect it while fabricating the vias for fluid inlet/outlet and electrical contacts. On the back of the wafer, a thick 6.2 μm of AZ-4562 photoresist was spin coated and patterned, followed by a deep etch-through of the silicon wafer. After obtaining the vias, the silicon wafer was diced into individual chips. A blank borosilicate glass wafer was also diced into chips of the same size, to be used as

covers for the device. The bonding of the glass covers to the silicon chips was performed in the BA-6 anodic bonding system (MicroSuss, Germany). After the bonding process, copper wires were contacted to the Cr/Au pads by filling the vias with a silver based epoxy resin. Fig. 2 shows the fabrication process, while Fig. 3 shows the final encapsulated device.

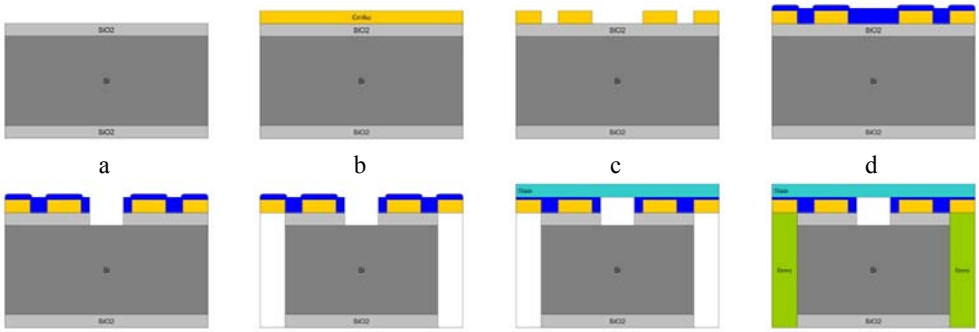

Fig. 2: The fabrication process of the device: a) growth of thermal silicon oxide; b) deposition of Cr/Au metal layer; c) etching of the metal layer; d) deposition of PECVD silicon oxide; e) etching of the microfluidic channel in the PECVD/thermal oxide; f) deep silicon etching of the vias; g) anodic bonding of glass and wafer; h) electrical contacting by conductive epoxy

Fig. 3: The final encapsulated device and a coin for size reference

3. Electromagnetic and electrothermal numerical simulations

Commercially available software COMSOL Multiphysics 4.1 and CoventorWare2010 were used to perform electrothermal and electromagnetic simulations. The material parameters taken into account for the simulations are shown in Table 1. For the simulated model we have taken into account all the materials used in the fabricated device. Electromagnetic simulations were performed in order to determine the magnetic induction generated by a 100 mA electrical current running through the conductive wires. The width of the wires is 20 μm at their thinnest and the thickness is 150 nm.

Table 1

Properties of the materials used in the fabrication

	Thermal conductivity [pW/μmK]	Specific heat [pJ/kgK]	Electrical conductivity [pS/μm]	Dielectric constant
Si	$1.57 \cdot 10^{8}$	$7.03 \cdot 10^{14}$		11.7
SiO_2	$1.422 \cdot 10^{6}$	$1.0 \cdot 10^{15}$		3.9
Au	$2.97 \cdot 10^{8}$	$1.287 \cdot 10^{14}$	$4.4 \cdot 10^{13}$	
Pyrex Glass	$1.4 \cdot 10^{6}$	$8.35 \cdot 10^{14}$		8.0
The relative magnetic permeability for all materials is: $\mu = 1$				

In the area of interest, the B_x component of the magnetic induction is constant, therefore it is considered to be negligible because the magnetophoretic effect is proportional to the magnetic induction gradient. As a consequence we will only refer to the B_y component of the magnetic induction. Fig. 4 shows the simulated B_y component of the magnetic induction. For a more relevant analysis of the simulation, the high values obtained close to the wires were excluded.

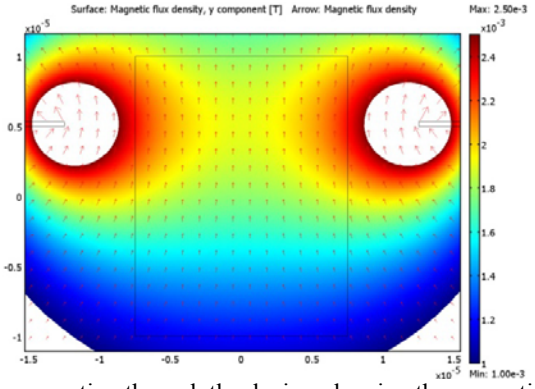

Fig. 4: 2D model, cross section through the device, showing the magnetic induction B_y. The central rectangle represents the microfluidic channel, while the two horizontal lines represent the metal wires. The scales on the left and bottom show the dimension of the simulated structure (scale $1:10^{-5}$ meters), while the colour chart shows the magnetic induction (in mT) The white circles are the results excluded in order to obtain a more detailed image of the magnetic field induction inside the microfluidic channel.

The simulated results show a magnetic induction gradient of about 50 T/m from the center of the microchannel to the sidewall, with an induction of about 2 mT in the center of the microchannel.

Electrothermal simulations were performed in order to determine the heat generated by the conductive wires. For the simulation of the heat distribution we have considered a voltage of 5 V applied on the electrical pads, which is equivalent to a current of 100 mA. Radiation and convection are applied as boundary conditions and are considered to be the exchange mechanisms with the surrounding environment. The temperature of the environment is considered to be

293 K (20°C), and the heat transfer coefficient in air is 20 W/m^{2}K. The physical interpretation of the boundary conditions is to assume the device is surrounded by air or placed on a thermal insulator. The boundary conditions used in the simulation represent the worst case scenario for the maximum working temperature.

Fig. 5 (left) shows the temperature distribution at the surface of the chip, if the entire stack of materials is taken into account, including the glass slide used to encapsulate the microfluidic channel. The temperature at the surface of the chip is about 40 K above environmental temperature. Fig. 5 (right) shows the temperature distribution on the conductive wires. The highest temperature, about 50 K above environmental temperature, is observed in the thinnest point of the wires.

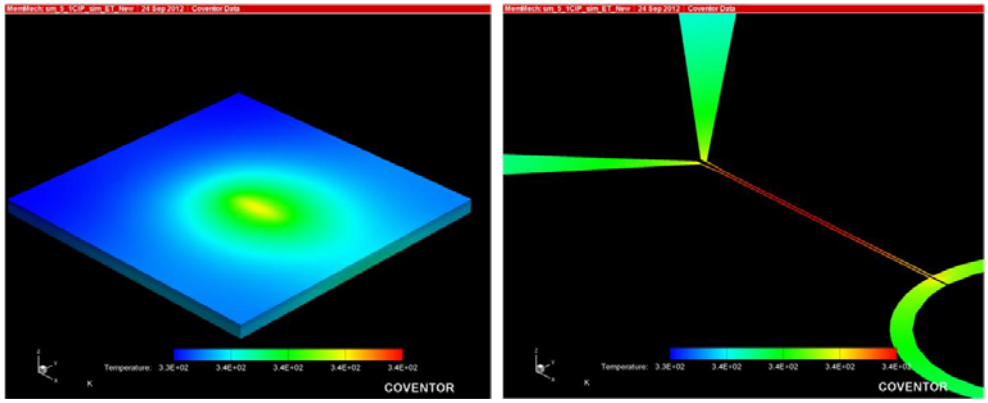

Fig. 5: On the left, the maximum temperature which can be attained at the surface of the system when a voltage of 5 V is applied. The full stack of materials is taken into account, including the glass slide used to encapsulate the microfluidic channel (Si, SiO2, Au, Glass).
On the right, the maximum temperature reached at the surface of the conducting wires.
The temperature colour bar runs from 330 K (dark blue) to 340 K (red)

4. Experimental set-up

To test the device, we synthesized maghemite nanoparticles, γ-Fe_2O_3. The synthesis starts with dissolving iron chloride ($FeCl_3 \bullet 6H_2O$) and iron sulfate ($FeSO_4 \bullet 7H_2O$) in deionized water. While the solution is continuously stirred, drops of ammonium hydroxide (NH_4OH 28%) are added. The precipitate is collected with a magnet and washed with deionized water.

To characterize the nanoparticles, we have plotted the magnetization curve using the 7T Mini-VSM (Cryogenic, UK). Fig. 6 shows the magnetization curve of the maghemite nanoparticles. The red line represents the Langevin fit. The interpretation of the measurements indicates an average magnetic diameter of 9.88 nm. [18] The hysteresis curve plotted from the Vibrating Sample Magnetometer

(VSM) measurements indicates the synthesized maghemite nanoparticles are superparamagnetic.

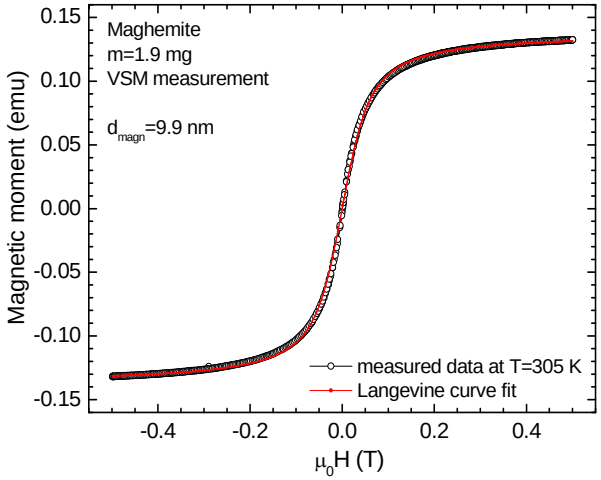

Fig. 6: The hysteresis curve plotted from the VSM measurements fitted by the Langevin function for 1.9 mg of maghemite nanoparticles at 305K

For the visualization of the magnetic nanoparticles in the microfluidic channel, we used an experimental setup comprised of an inversed microscope, a digital camera and a constant current source. The magnetophoretic devices were placed on an electrical insulating mount, on top of the microscope objective. The maghemite nanoparticles solution was flown through the device using capillary flow. Fig. 7 shows the experimental set-up and the placement of the sample on the insulated mount.

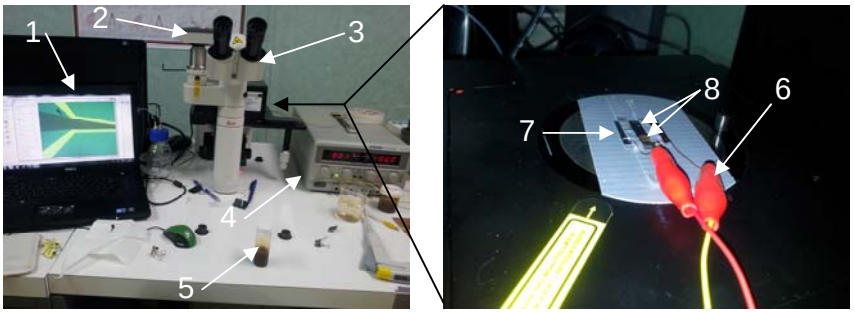

Fig. 7: The experimental set-up: 1) laptop for recording images; 2) digital camera; 3) inversed microscope; 4) constant current source; 5) maghemite nanoparticles solution; 6) electrical connectors to the constant current source; 7) magnetophoretic device fixed on the insulated microscope mount; 8) fluid inlet/outlet orifices

5. Results and discussions

The fluid with suspended maghemite nanoparticles was introduced by adding droplets on the inlet of the microfluidic channel, the initial flow being obtained by capillary effect. After the microfluidic channel was filled, an electrical current was applied to the contacting pads. We observed leakage issues, fluid spilling outside the fabricated channel all over the insulated conductive wires. This might be due to improper surface cleaning before performing the anodic bonding between the silicon substrate and glass cover. Fig. 8 shows images captured during the experiment.

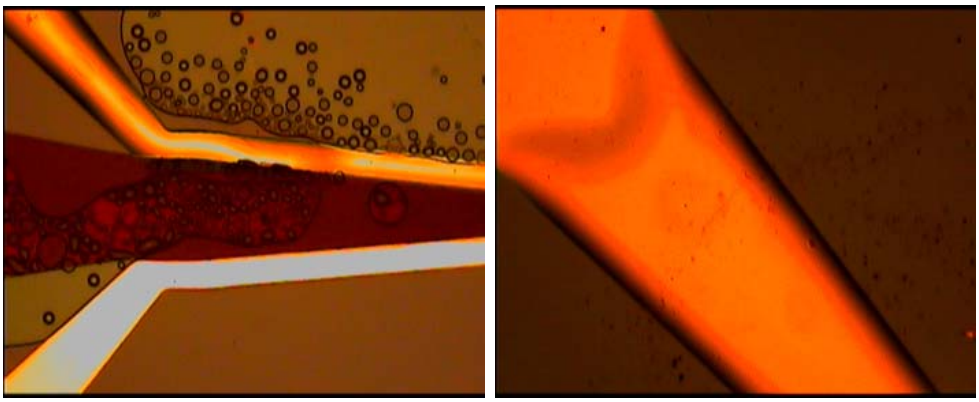

Fig. 8: On the left, a close up image of the area where the two conductive wires come in close vicinity to the fluid flow. Nanoparticle agglomerations can be observed close to the wires. On the right, an image of the conductive wire leading to the contacting pad. As fluid spilled out of the microfluidic channel, nanoparticles are agglomerated on the sides of the wire. In both images, the agglomerations appear as black areas and dots.

The magnetic field was generated by applying a constant current through the conductive wires. The current was gradually increased starting from 10 mA up to 150 mA. During the experiments, we observed the burn out of the electrical wires around 200 mA. The experiments we were force to limit the current through the wires to 150 mA, to ensure the integrity of the device.

By increasing the current to 30 mA we were able to observe the maghemite nanoparticles agglomerate. As the current reached 50 mA, the nanoparticle agglomerations started to move towards the sidewalls of the microfluidic channel. Continuing to increase the current resulted in more particles agglomerating and moving towards the side walls faster. Although our numerical simulations show a magnetic induction between 2 mT and 2.4 mT inside the microfluidic channel, while the synthesized maghemite nanoparticles reach magnetic saturation at roughly 300 mT, we were still able to observe the magnetophoretic effect. This is a direct result of the agglomerations of

nanoparticles. Without the presence of a magnetic field, the superparamagnetic nanoparticles have no magnetic moment. As the magnetic induction is increased, the magnetic moment of each nanoparticle increases, and the particles start interacting with their neighbors leading to the formation of clusters. The magnetic moment of each particle adds to the total magnetic moment of the cluster, which continues to increase as more nanoparticles are attracted by the agglomeration. We believe this is the main mechanism involved in the observed results.

Reaching 100 mA, the temperature in the microfluidic channel starts to play an important role, the thermo-capillary convection being observed. As the current is increased the heat output from the conductive wires creates temperature gradients between the cooler areas next to the inlet/outlet orifices and the heated microfluidic channel. This result in the formation of water droplets inside the fluid flow, which move along the microfluidic channel and drag along the maghemite nanoparticles trapped at the sidewalls. The effect limited the visualization of the magnetophoretic effect at higher currents, as the nanoparticles were not able to freely move under the influence of the magnetic field.

6. Conclusions

The results presented in this paper show the possibility of obtaining a magnetophoretic effect even at low magnetic fields and for electrical currents as low as 50 mA. This novelty of the design is the embedding of the conductive wires which induce the magnetic field in the sidewalls of the microfluidic channels, allowing the device to attract superparamagnetic particles even at low magnetic induction. An advantage of this proof-of-concept is the compatibility of the fabrication process with the ICT fabrication, allowing the integration of the devices with MEMS-NEMS devices, provided the temperature issue is solved.

R E F E R E N C E S

[1] *M.Zborowski, C.B.Fuh, R.Green, L.Sun, J.J.Chalmers*, "Analytical Magnetophoresis of Ferritin-Labeled Lymphocytes", Analytical Chemistry, vol. 67, no. 20, 1995, pp. 3702-3712

[2] *F.Assi, R.Jenks, J.Yang, C.Love, M.Prentiss*, "Massively parallel adhesion and reactivity measurements using simple and inexpensive magnetic tweezers", Journal of Applied Physics, vol. 94, no. 9, 2002, pp. 5584-5586

[3] *F.Amblard, B.Yurke, A.Pargellis, S.Leibler*, "A magnetic manipulator for studying local rheology and micromechanical properties of biological systems", Review of Scientific Instruments, vol. 67, no. 3, 1996, pp. 818-827

[4] *T.T.Hansel, I.J.M.Devries, T.Iff, S.Rihs, M.Wandzilak, S.Betz, K.Blaser, C.Walker*, "An Improved Immunomagnetic Procedure for the isolation of highly purified human blood eosinophils", Journal of Immunolgical Methods, vol. 145, no. 1-2, 1991, pp. 105–110

[5] *S.Miltenyi, W.Muller, W.Weichel, A.Radbruch*, "High-gradient magnetic cell-separation with MACS", Cytometry, vol. 11, no. 2, 1990, pp. 231–238

[6] *J.J.Chalmers, M.Zborowski, L.P.Sun, L.Moore*, "Flow through, immunomagnetic cell separation", Biotechnology Progress, vol. 14, no. 1, 1998, pp. 141–148
[7] *C.H.Ahn, M.G.Allen*, "A fully integrated micromachined magnetic particle manipulator and separator", in Proceedings IEEE Micro Electro Mechanical Systems An Investigation of Micro Structures, Sensors, Actuators, Machines and Robotic Systems, 1994, pp. 91-96
[8] *C.H.Ahn, M.G.Allen, W.Trimmer, Y-N.Jun, S.Erramilli*, "A fully integrated micromachined magnetic particle separator", J. of Microelectromech. Syst., vol. 5, 1996, pp. 151-158
[9] *J.Do and C.H.Ahn*, "A Functionally Dynamic Microchamber with Rapid Mixing and Reaction Capabilities for Magnetic Bead-Based Immunoassay", Proceedings of the 8th International Conference on Micro Total Analysis Systems (micro-TAS 2004), Malmo, Sweden, vol. 2, September 26-30, 2004, pp. 416-418
[10] *Q.Ramadan, D.Poenar, V.Samperb, C.Yu*, "Magnetic-based microfluidic platform for biomolecular separation", Biomedical Microdevices, vol. 8, no. 2, 2006, pp. 151-158
[11] *R.Wirix-Speetjens, W.Fyen, J. de Boeck, G.Borghs*, "Enhanced magnetic particle transport by integration of a magnetic flux guide: Experimental verification of simulated behaviour", Journal of Applied Physics, vol. 99, no. 8, 2006
[12] *E.Mirowski, J.Moreland, S.E.Russek, M.J.Donahue*, "Integrated microfluidic isolation platform for magnetic particle manipulation in biological systems", Applied Physics Letters, vol. 84, no. 10, 2004, pp. 1786-1788
[13] *N.Pamme, C.Wilhelm*, "Continuous sorting of magnetic cells via on-chip free-flow magnetophoresis", Lab on a Chip, vol. 6, 2006, pp. 974–980
[14] *D.W.Inglis, R.Riehn, R.H.Austin, J.C.Sturm*, "Continuous microfluidic immunomagnetic cell separation", Applied Physics Letters, vol. 85, 2004, pp. 5093–5095
[15] *K.S.Kim, J-K.Park*, "Magnetic force-based multiplexed immunoassay using superparamagnetic nanoparticles in microfluidic channel", Lab on a Chip, vol. 5, no. 6, 2005, pp. 657-664
[16] *C.Iliescu, G.Xu, E.Barbarini, M.Avram, A.Avram*, "Microfluidic device for continuous magnetophoretic separation of white blood cells", Microsystem technologies micro and nanosystems-information storage and processing systems, vol. 15, 2009, pp. 1157–1162
[17] *M.Volmer, M.Avram*, „Micromagnetic Simulations on Detection of Magnetic Labeled Biomolecules Using MR Sensors", Journal of Magnetism and Magnetic Materials, vol. 321, 2010, pp. 1683-1685
[18] *M.Volmer, M.Avram*, „Microbeads Detection Using Spin-Valve Planar Hall Effect Sensors", Journal of Nanoscience and Nanotechnology, vol. 12, no. 1–4, 2012